LA-UR- 09-00169

Approved for public release;
distribution is unlimited.

Title:	Detonation Propagation in a High Loss Configuration
Author(s):	Scott I. Jackson and Joseph E. Shepherd
Intended for:	22nd International Colloquium on the Dynamics of Explosions and Reactive Systems, Minsk, Belarus, July 27-31 2009

Form 836 (7/06)

Detonation Propagation in a High Loss Configuration

Scott I. Jackson[1], Joseph E. Shepherd[2]

[1]Los Alamos National Laboratory, Los Alamos, NM 87507, USA

[2]GALCIT, California Institute of Technology, Pasadena, CA, 91125, USA

1 Introduction

This work presents an experimental study of detonation wave propagation in tubes with inner diameters (ID) comparable to the mixture cell size. Propane-oxygen mixtures were used in two test section tubes with inner diameters of 1.27 mm and 6.35 mm. For both test sections, the initial pressure of stoichiometric mixtures was varied to determine the effect on detonation propagation. For the 6.35 mm tube, the equivalence ratio ϕ (where the mixture was ϕ C_3H_8 + $5O_2$) was also varied. Detonations were found to propagate in mixtures with cell sizes as large as five times the diameter of the tube. However, under these conditions, significant losses were observed, resulting in wave propagation velocities as slow as 40% of the CJ velocity U_{CJ}. A review of relevant literature is presented, followed by experimental details and data. Observed velocity deficits are predicted using models that account for boundary layer growth inside detonation waves.

2 Previous Relevant Work

In published literature, several different modes of detonation wave propagation below the CJ wave velocity have been observed including sub-CJ detonation waves, low-velocity detonation waves, and galloping waves. A brief description of each mode and a summary of relevant literature is given below.

Mode	Propagation Velocity	Reference
Overdriven detonation	> 1.00 U_{CJ}	Sharpe (2001)
Typical detonation	0.90 - 1.00 U_{CJ}	Lewis and von Elbe (1961)
Sub-CJ detonation	0.70 - 0.90 U_{CJ}	Paillard et al. (1979)
Low-velocity detonation	0.45 - 0.60 U_{CJ}	Manzhalei (1999)
Galloping detonation	0.50 - 1.50 U_{CJ}	Lee et al. (1995)

Table 1: Observed detonation propagation velocities.

Correspondence to : sjackson@lanl.gov

2.1 Detonations and Sub-CJ Detonations

Detonations and sub-CJ detonations propagate at velocities at or slightly below U_{CJ}, but are still thought to have a sonic surface behind the leading shock wave (Brailovsky and Sivashinsky, 2000). The sonic surface is a region of flow behind the reaction zone where the flow becomes locally sonic. Thus, the detonation wave is supersonic relative to products behind the sonic surface and disturbances behind the sonic surface cannot affect the wave propagation. However, disturbances in front of the sonic surface are expected to affect the detonation propagation.

Kistiakowsky et al. (1952a) experimentally observed that decreasing the tube diameter resulted in a decrease in detonation velocity in cyanogen-oxygen mixtures. Four different tube inner diameters were used (10, 5, 2.5, and 1.2 cm) with two different cyanogen-oxygen mixtures. The initial pressure was not reported but is assumed to be 1 atm. The smallest diameter tube exhibited a 3% detonation velocity decrease when compared to the largest diameter tube. Other studies by Kistiakowsky et al. (1952b) and Kistiakowsky and Zinman (1955) observed velocity deviations from CJ of up to 2% in acetylene-oxygen mixtures with varying tube diameters.

Fay (1959) attributed these velocity differences to boundary layer growth in the detonation wave resulting in flow divergence behind the shock wave. This flow divergence causes less energy to be released in the reaction zone before the sonic state is attained, underdriving the detonation wave and causing wave propagation at a decreased velocity. Fay developed a model to quantify this boundary layer effect and found that the model agreed well with selected experimental data from Kistiakowsky and Zinman (1955).

Dove et al. (1974) extended Fay's model by computing velocity deficits in small diameter tubes using a quasi-one-dimensional ZND model with reaction kinetics and allowing for cross-sectional area changes in the flow. Hydrogen-oxygen gas mixtures were investigated and numerical results were compared with experimental data. It was found that the computational results underpredicted the measured velocity deficits.

Paillard et al. (1979) investigated hydrogen azide detonations in 1, 2, 5, and 10 mm ID tubes over a pressure range of 1-25 torr. Deficits of 30% were observed at the lowest pressures in the smallest diameter tubes. Wall heat fluxes were also recorded. For larger tubes and higher pressures, it was found that the CJ theory modeled the flow well; however, near propagation limits, the theory failed. They concluded that, in order to explain the velocity deficits, it was necessary to take into account kinetic parameters in the detonation structure.

Vasil'ev (1982) constructed an experiment capable of simultaneously measuring the detonation velocity in several differently sized rectangular channels. His study was primarily concerned with establishing detonation limits in stoichiometric hydrogen-oxygen and acetylene-oxygen mixtures, and detonation failure was assumed to occur at the onset of the galloping regime. However, one of his streak camera photographs appears to have captured a sub-CJ detonation, a low-velocity detonation, and a galloping wave propagating relative to each other in separate channels.

Dupre et al. (1986) studied the propagation of marginal detonations in lean hydrogen-air mixtures using a facility consisting of five tubes of decreasing diameter connected by 180° bends. The design was such that marginal waves propagating through the experiment would eventually fail as the wave propagated through increasingly smaller diameter tubing. Velocity deficits of up to 10% were observed. Dupre et al. (1986) attempted to fit the experimental data with a model based on the work of Fay (1959) and Dabora (1963) and found that the experimental data had a large amount of scatter but generally followed the same trend as the model. The scatter in the data was probably due to the presence of 180° bends and short sections of Shchelkin spiral used in between tube diameter transitions.

In numerical work, Zel'dovich et al. (1987) added friction and heat loss terms to the equations of motion to model losses behind the detonation wave. Using the extended ZND theory, they calculated the effect of the friction on the flow. Their results were qualitative; however, they did note that detonation velocity decreased with increased friction. Frolov and Gelfand (1991) and Agafonov and Frolov (1994) also used frictional and heat losses to model tube size effects and predict detonation limits.

2.2 Low-Velocity Detonations

Low-velocity detonations have the lowest propagation velocity of any observed detonations and consist of a complex composed of a leading shock wave followed by a flame, which maintains a constant distance behind the shock front. While flame propagation velocities in quiescent gas are typically much slower (by several hundred meters per second) than the shock propagation velocity, the flame in the complex propagates into gas which has been accelerated by the shock wave. Thus, for the flame to remain a fixed distance behind the shock wave, the sum of the flame speed (in a quiescent mixture) and the post-shock flow velocity must equal the shock propagation velocity.

Manzhalei (1999) notes that in this situation, tube walls will induce a boundary layer in the post-shock flow. Discussed in detail in Section 4.1, the boundary layer growth removes mass from the freestream flow and forces it to expand as if the tube walls were diverging. This expansion results in decreasing post-shock flow velocity with increasing distance from the shock wave and allows the flame to stabilize some distance behind the wave. While low-velocity detonations are supersonic with respect to the reactant mixture, the post-shock flow is entirely subsonic. This is in contrast to the sonic condition present at the end of a CJ detonation wave.

Experiments by Manzhalei (1992, 1999) observed a low-velocity detonation regime while propagating detonations through capillary tubes with diameters of 0.6, 1.0, and 2.1 mm in stoichiometric acetylene-oxygen gas mixtures by using a photomultiplier to detect chemiluminescence. Wave velocities as low as 0.50 U_{CJ} were measured for initial pressures of 0.05 atm in the 0.6 mm tube. These velocities were so low that he did not believe that ignition from adiabatic shock compression alone was possible and, instead, attributed the chemiluminescence to a deflagration or flame trailing behind the shock wave. The location of the luminous front was determined to exist at a constant value ranging from three to eight tube diameters behind the preceding shock wave.

Manzhalei also found that the low-velocity detonation regime and the more typically observed multifront detonation regime were separated by an additional regime characterized by galloping detonation waves. He observed that the boundary between the low-velocity regime and the galloping regime exists when the induction time of the shocked gas equals the time necessary for the gas to travel between the shock wave and flame front.

Numerical simulations by Brailovsky and Sivashinsky (2002, 2000) have used friction factors and heat loss terms to develop a model that solves for sub-CJ detonations, low-velocity detonations, and subsonic combustion. Their model solves for sub-CJ detonations using the ZND equations and a generalized CJ condition, which assumes that the solution remains nonsingular through the sonic surface. When, as in the case of the low-velocity detonation regime, the CJ criterion cannot be satisfied, Brailovsky and Sivashinsky (2002) instead assumed that the absolute particle velocity is zero at the end of the reaction zone in order to obtain a solution.

Simulations by Dionne et al. (2000) further investigated the effect of using a friction source term in the momentum equation. They solved the steady ZND structure with the generalized CJ criterion and used the criterion of Brailovsky and Sivashinsky (2000) to solve for the flow when the generalized CJ criterion could no longer be met. They also performed unsteady numerical simulations in the low-velocity detonation regime. Both Dionne et al. (2000) and Brailovsky and Sivashinsky (2000) determined the detonation velocity deficit as a function of flow friction, or drag, and found that multiple detonation velocities were possible for some unique values of friction.

Quasi detonations in tubes with dense obstacle fields along the tube wall have been experimentally measured to propagate as slowly as 0.40 U_{CJ} (Teodorczyk et al., 1988). The detonation wave was observed to fail as it diffracted around each obstacle and then to reinitiate after reflecting from the tube wall. It was unclear whether the reinitiation was due to autoignition of gas behind the reflection of the failing wave or due to vortex mixing in this region; however, in experiments where this wave reflection was damped by wire mesh, reinitiation was not observed. Strictly speaking, it may not be valid to classify these results as low-velocity detonations or sub-CJ detonations since the wave continuously fails and reinitiates rather than propagating at a relatively constant, yet diminished, velocity. However, in

a global sense, the waves in each experiment (Teodorczyk et al., 1988) were observed to propagate at average velocities below that of U_{CJ}.

2.3 Galloping Detonations

Galloping detonations are characterized by detonation propagation velocities that oscillate between a low (0.5 U_{CJ}) and a high (1.5 U_{CJ}) velocity. The end result is average wave speeds between 0.8 - 1.0 U_{CJ}. The typical oscillation period is on the order of 100 tube diameters so it is possible for measurements with insufficient resolution to misidentify galloping detonations as underdriven stable detonations.

Edwards et al. (1970) used a microwave interferometer to observe propagation of such detonations in large-aspect-ratio rectangular channels (76 mm $\times$ 6.4 mm $\times$ 6 m long). Using the wave velocity as a measure of stability, they found that it was necessary to observe the waves over long distances to ensure that they were stable and would not fail. In particular, their facility required about 100 tube widths to damp out the overdrive from their initiator and another 100 tube widths to determine the stability of the marginal wave. Edwards et al. (1971) continued the research, using the microwave interferometer in a rectangular (23 mm $\times$ 10 mm $\times$ 30 m) channel to obtain finely resolved velocity measurements of "cyclic-velocity" or galloping waves.

More detailed interferometry work on detonations was conducted by Lee et al. (1995), who tested and characterized a large number of hydrocarbon mixtures using high-resolution velocity measurements in tubes. Several modes of detonation propagation were identified including stable detonations, rapidly fluctuating detonations, stuttering detonations (a mild form of galloping detonations), galloping detonations, low-velocity stable detonations, and failed detonations. Stable low-velocity, the slowest observed mode of detonation propagation, traveled at speeds as low as 0.5 U_{CJ}. Similar low-velocity wave propagation (0.5 U_{CJ}) was also observed in interferometry work by Haloua et al. (2000), who classified these waves as fast flames.

2.4 Shock Waves in Small Diameter Tubes

Work by Brouillette (2003) on shock wave propagation in small diameter tubes has shown that viscous and heat losses to the wall can significantly affect the flow. He developed shock jump conditions that included terms for shear stresses and heat flux at the wall and found that when solving the jump conditions for a given Mach number, accounting for momentum and heat losses resulted in higher post-shock pressures and lower particle velocities than flows with no losses. Experiments conducted in a small-scale shock tube qualitatively agreed with his model and demonstrated the importance of considering loss terms when working in such small scales.

3 Experimental Setup

The experiment consisted of an initiator tube attached to a smaller diameter test section tube. The initiator tube (Schultz, 2000) had a 38.1 mm ID and was 1.5 m long. One end flange of the detonation tube contained a spark plug connected to an electric-discharge system with 30 mJ stored energy. A 30.5 cm long section of Shchelkin spiral with a wire diameter of 4 mm and a coil spacing of 11 mm was located just downstream of the spark plug to promote DDT. The initiator tube contained two PCB pressure transducers (model 113A26) that were spaced 0.42 and 0.82 m from the ignition point in order to detect that a detonation was successfully initiated. The transducer closest to the ignition point was referred to as P0 and the further one was referred to as P1.

The initiator-tube end flange opposite the spark plug was connected to the smaller diameter test section tube. Two different test section tubes (1.27 mm and 6.35 mm ID) were used and are described below. Each test section tube protruded some distance (given below) into the initiator tube in a cookie-cutter-style setup to mitigate the effects of wave reflection off the initiator tube end flange. Each test section tube was fitted with four PCB pressure transducers (model 113A26) to facilitate wave speed and

pressure measurements. The transducers were labeled P2, P3, P4, and P5 with increasing distance from the spark point.

Prior to each run, the initiator and test section tubes were evacuated below a pressure of 0.2 mbar and then filled with the test mixture using the method of partial pressures. To ensure mixture homogeneity, the mixture was recirculated in the experiment for 15 minutes prior to each run using a bellows-style pump.

3.1 1.27 mm Inner Diameter Test Section

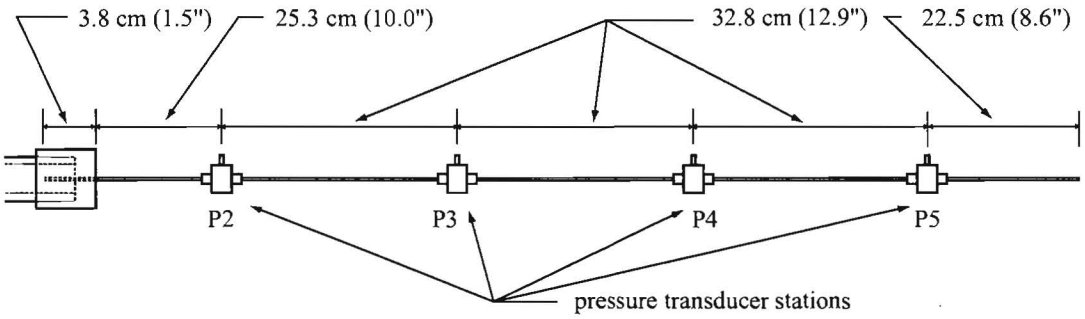

Figure 1: Relevant dimensions of the 1.27 mm ID test section are shown. The end of the initiator tube is shown on the left side of the figure. A more detailed drawing of the pressure transducer station is shown in Fig. 2.

A schematic of the 1.27 mm ID test section is shown in Fig. 1. It consisted of five sections of 1.27 mm ID stainless steel tubing (3.18 mm outer diameter) interrupted by pressure transducer stations. The total length of the test section was 1.50 m, corresponding to 1181 tube diameters. Each tube length was 25.4 cm long and connected to pressure transducer stations using Swagelok fittings. The total distance in between each pressure transducer, accounting for the length of the fittings, was 32.8 cm.

Each pressure transducer station was 25 mm long with an ID of 3.20 mm. A 0.76 mm diameter hole located in the middle of each section was connected to a pressure transducer. Due to machining constraints, there were other ID variations in the pressure transducer station that are illustrated in the enlarged view in Fig. 2. The 1.27 mm ID test section protruded 3.8 cm into the initiator tube.

Stoichiometric propane-oxygen mixtures were used during testing of the 1.27 mm ID tube. Initial pressures of those mixtures ranged from 0.13 to 1.80 bar. Lower pressures were tested as well, but detonation initiation did not occur below 0.13 bar.

3.2 6.35 mm Inner Diameter Test Section

The 6.35 mm ID test section (Fig. 3) consisted of an uninterrupted length of steel tubing 1.82 m long (287 tube diameters). Four pressure transducers were spaced 0.508 m apart and measured the pressure through 1.5 mm diameter holes drilled in the tube wall. The 6.35 mm test section protruded about 10 cm into the initiator tube.

Propane-oxygen mixtures were tested in the 6.35 mm test section. For stoichiometric mixtures, the pressure was varied from 0.15 to 1.00 bar. The equivalence ratio of the propane-oxygen mixture was also varied from 0.3 to 3.0 while keeping the initial pressure fixed at 1.00 bar.

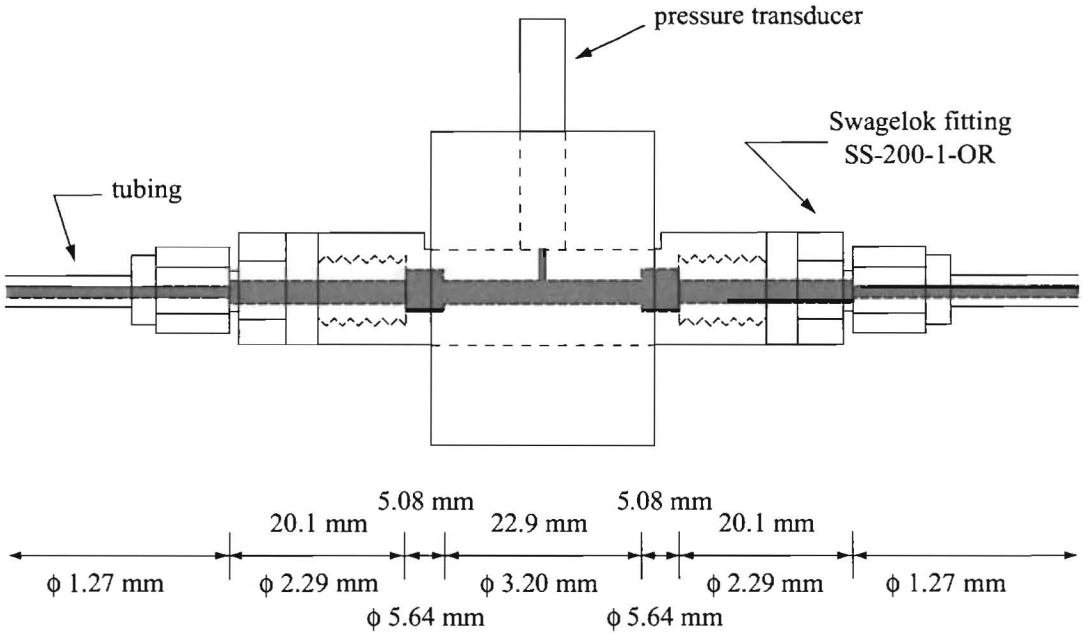

Figure 2: An enlarged drawing of the 1.27 mm ID tube pressure transducer station is shown. The volume filled with combustible mixture is shaded grey and the dimensions given correspond to this volume.

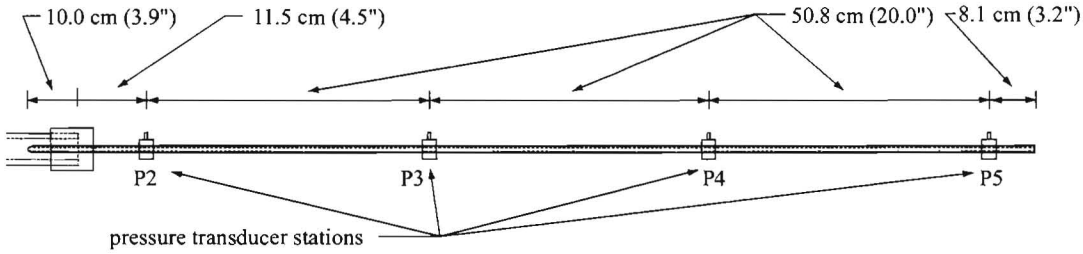

Figure 3: Relevant dimensions of the 6.35 mm ID test section are shown. The end of the initiator tube is on the left side of the figure. An enlarged view of the pressure transducer is not shown because there were no internal diameter changes in this test section.

4 Analysis and Theory

The average wave velocity in between each pressure transducer station was calculated by dividing the distance between adjacent stations by the difference in the arrival times of the wave. Since there were four pressure transducer measurements in the test section, this technique yielded three velocity measurements in the test section for each run. These velocity data are normalized by U_{CJ} and appear in Fig. 4a for varying initial pressure and 4b for varying equivalence ratio. Averaging these three velocity measurements for each experiment produced an average test section velocity U_{AVG} (Figs. 4c and 4d).

Values of U_{CJ} were calculated using the equilibrium code STANJAN REFReynolds (1986).

The data from varying equivalence ratio in the 6.35 mm ID tube (Figs. 4b and 4d) show small velocity deficits less than 10% as the mixture composition diverges from stoichiometric and the induction zone length Δ (the distance between the shock front and the reaction zone) increases. As the initial pressure in the 6.35 mm ID tube is decreased (Fig. 4a and 4c), small velocity deficits are also observed until the initial pressure is decreased to 0.10 bar. At the lowest pressure tested (0.10 bar), a significant decrease in wave velocity (0.65 U_{CJ}) exists. Experiments in the 1.27 mm ID tube display dramatic velocity deficits (up to 59%) as initial pressure is decreased. The detonation velocity smoothly decreases with decreasing pressure and the minimum wave propagation velocity measured was 0.41 U_{CJ} for an initial pressure of 0.14 bar.

Examples of the pressure transducer histories are shown in Fig. 5a for the 6.35 mm tube with $U_{AVG}/U_{CJ} = 1.01$ and in Fig. 5b for $U_{AVG}/U_{CJ} = 0.42$. Both sets of traces show the characteristic pressure signature of a detonation wave near the exit of the initiator tube. The actual presence of a detonation is difficult to verify, however, since no diagnostics were used to detect the reaction zone in these experiments and a combustion-driven shock wave could have a similar appearance. However, the velocity deficit smoothly increases as mixture sensitivity decreases, indicating that the detonation wave is experiencing increased losses rather than failure. Detonation failure at some limiting value would appear as a discontinuous decrease in the test-section velocity as a function of Δ/R, which is not observed in the data.

Fig. 4 indicates that the wave velocity deficits increase as ϕ varies from unity, with decreasing initial pressure, and with decreasing tube diameter. Decreasing pressure and varying ϕ from unity tend to increase Δ. The dependence of the velocity deficits on Δ and the tube diameter are more clearly illustrated by replotting all experimental data as a function of induction zone length normalized by the inner tube radius R (Fig. 6a).

The induction zone lengths for each data point were calculated by first assuming that mixtures were adiabatically compressed and accelerated by a shock wave propagating at the experimentally measured wave speed and then allowed to undergo constant volume combustion. For all calculations, the induction zone length was defined as the product of the post-shock fluid velocity (in shock-fixed coordinates) and the time when the temporal temperature gradient was 90% of the peak value. The shock-jump conditions were numerically solved using the equilibrium code STANJAN (Reynolds, 1986) and the time for constant volume combustion was solved with the computer program CV (Shepherd, 1986) which uses the Chemkin package (Kee et al., 1989).

The data appear to collapse to a single relationship suggesting that

$$\frac{U}{U_{CJ}} = f\left(\frac{\Delta}{R}\right) \tag{1}$$

as shown in Fig. 6a, although closer examination shows a discontinuous step located near $\Delta/R = 0.1$ that separates the 6.35 mm ID tube data (characterized by low-velocity deficits) and the 1.27 mm ID tube data (characterized by high-velocity deficits). However, one data point from the 6.35 mm ID tube is located among the 1.27 mm ID tube data near $\Delta/R = 100$.

4.1 Boundary Layer Growth

A shock wave propagating through a tube will impulsively accelerate the gas that it processes. If the post-shock gas velocity is different than that of the tube wall and the no-slip condition holds for the gas, viscous forces will accelerate the gas closest to the wall to match the wall velocity. The flow unaffected by the no-slip boundary condition is independent of the Reynolds number and is referred to as the freestream flow. The viscous or momentum boundary layer is defined as the region of gas that is affected by the wall and will grow in size as the wall momentum diffuses into the freestream fluid. Thermal differences between the freestream fluid and the wall will also result in the growth of a thermal

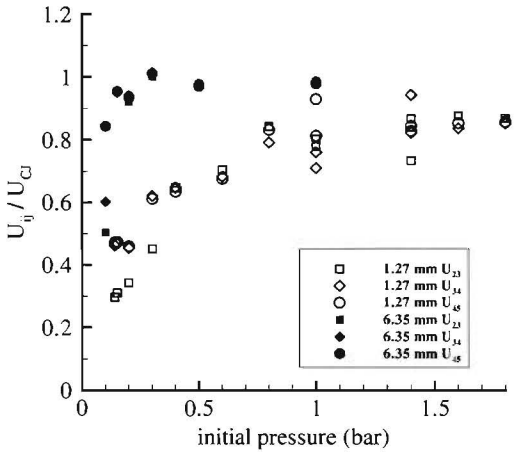

(a) Velocity in between each measurement station versus initial pressure.

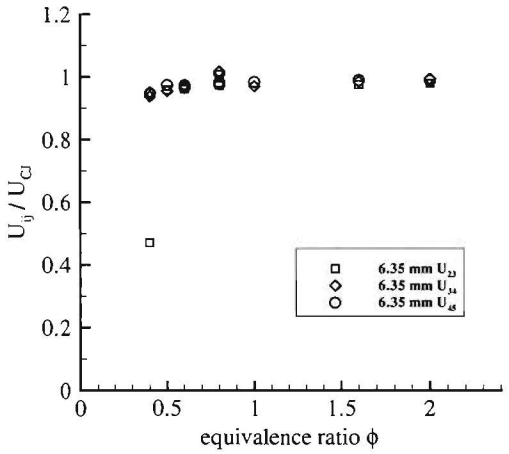

(b) Velocity in between each measurement station versus equivalence ratio.

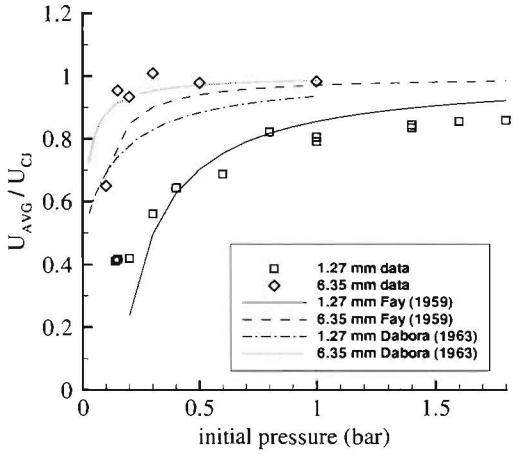

(c) Average test section velocity versus initial pressure.

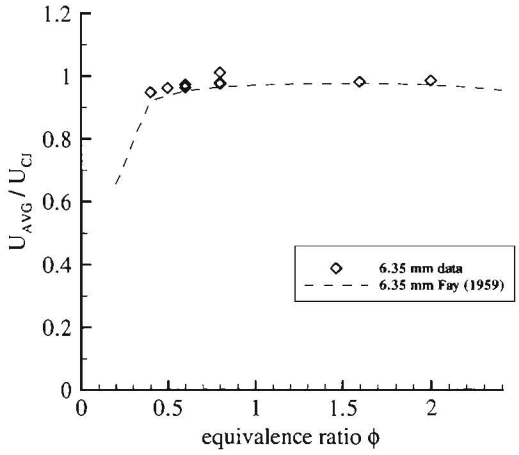

(d) Average test section velocity versus equivalence ratio.

Figure 4: Test section velocity data: Average wave velocity in between each pressure measurement station is shown for (a) varying initial pressure and (b) varying equivalence ratio. U_{ij} is the average velocity between pressure transducers i and j. The individual wave speeds from each run in (a) and (b) have been averaged resulting in a single average test section velocity for each run as shown in (c) and (d). The lines correspond to the models in REFFay (1959) and REFDabora (1963) that account for boundary layer effects.

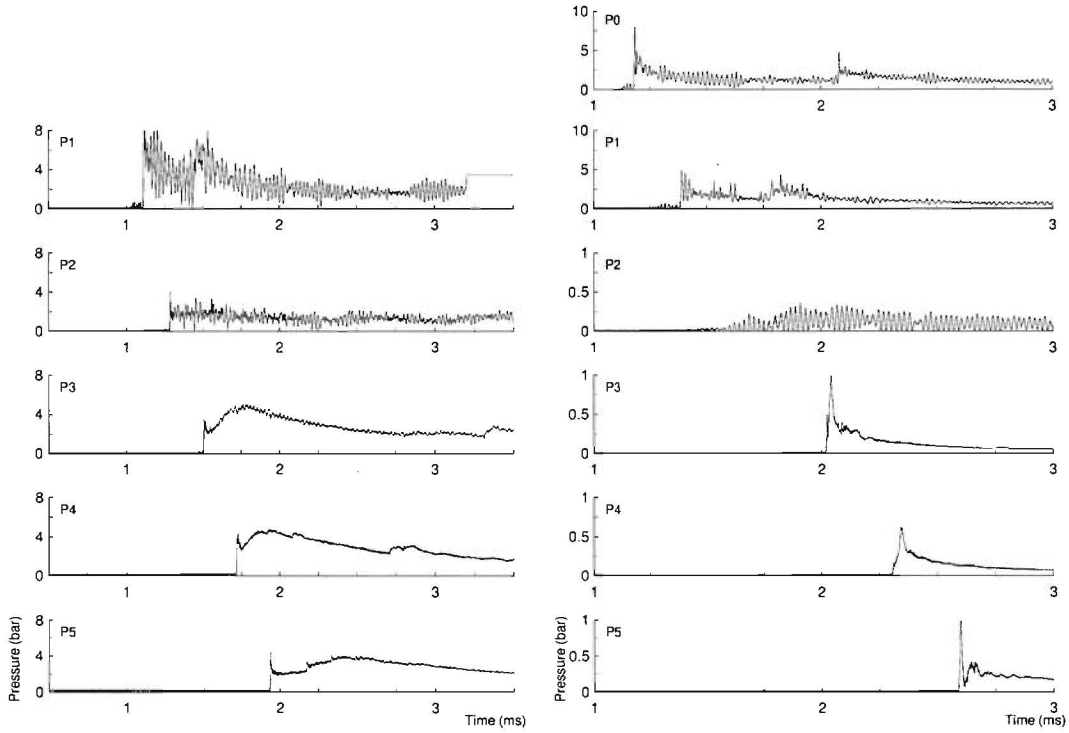

(a) Shot 016: $C_3H_8+5O_2$ with $P_1 = 0.30$ bar in 6.35 mm ID tube. Average test section velocity was 1.01 U_{CJ}.

(b) Shot 045: $C_3H_8+5O_2$ with $P_1 = 0.15$ bar in 1.27 mm ID tube. Average test section velocity was 0.42 U_{CJ}.

Figure 5: Examples of pressure traces from both test sections.

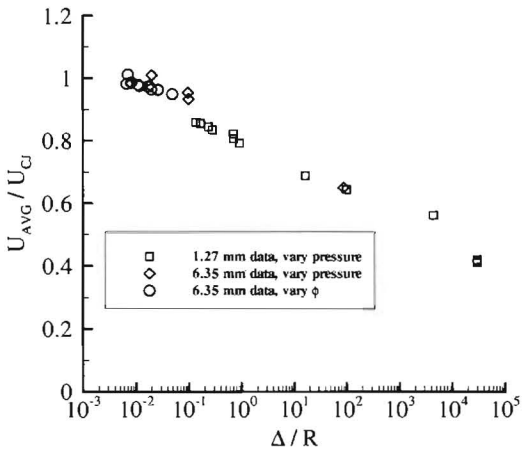

(a) All experimental velocity data.

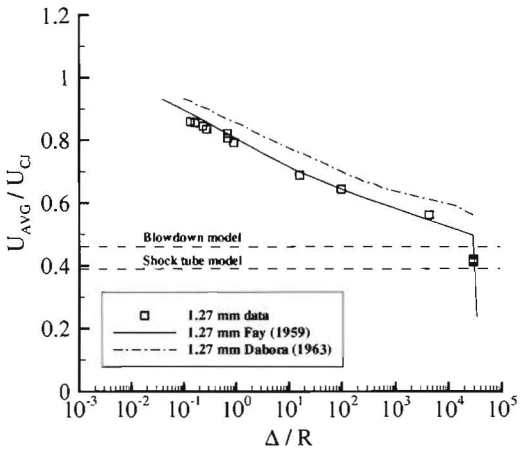

(b) Data from varying pressure in the 1.27 mm ID tube.

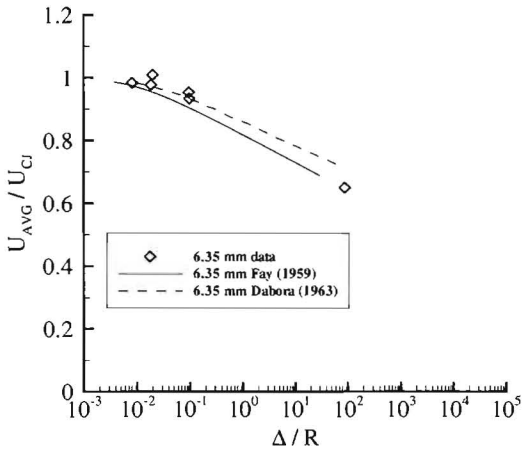

(c) Data from varying pressure in the 6.35 mm ID tube.

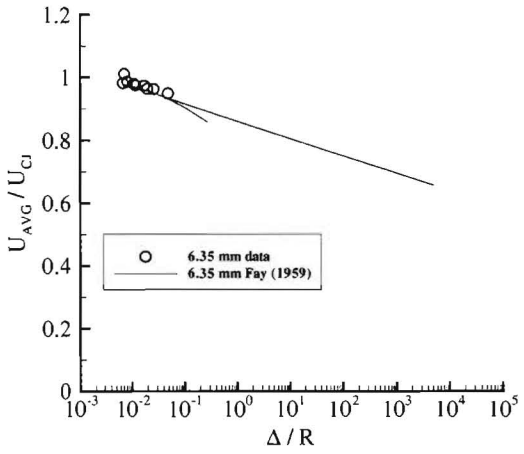

(d) Data from varying ϕ in the 6.35 mm ID tube.

Figure 6: Experimental data presented as a function of induction zone length Δ normalized by tube radius. The lines correspond to boundary layer models discussed in the text.

boundary layer. The momentum and thermal boundary layers typically grow at similar rates in gases due to their comparable diffusivities of momentum and heat transport.

Fig. 7 illustrates the velocity and temperature profiles behind a shock propagating in a tube filled with gas that is initially moving at the same velocity as the wall. As the flow enters the viscous boundary layer, it is accelerated towards the wall velocity. As the flow enters the thermal boundary layer, its temperature approaches the tube wall temperature. If the fluid and tube wall were initially at similar temperatures, the shock-processed gas would initially be much hotter than the tube wall and would cool isobarically (as there is no mechanism to support a pressure difference between the freestream and boundary layer flow) upon entering the thermal boundary layer. Thus, gas entering the boundary layer will increase in density, as per the ideal gas law.

These velocity and density changes cause gas entering the boundary layer to contract, forcing the freestream gas to expand to match the pressure at the interface between the boundary layer and the freestream fluid. The end result is that mass appears to be drawn from the flow into the tube wall or that the apparent flow area behind the shock front diverges. This apparent wall-sink effect can be modeled as a negative displacement thickness δ^* growing behind the shock and is primarily due to the velocity change, although the density change contributes to the effect as well. The shock accounts for this effect by curving near the tube wall to direct flow radially into the wall.

The boundary layer growth can be important to detonation propagation. Shocked gas that enters the thermal boundary layer before autoigniting will undergo a significant temperature reduction that can delay or eliminate autoignition altogether. Furthermore, the flow divergence induced by the momentum boundary layer will expand the flow and slow the rate of energy release during combustion. As the energy release is slowed, more energy is released behind the sonic surface. Energy released behind this surface is not able to propagate upstream and does not contribute to the detonation wave propagation.

These thermal and momentum losses become more significant as the ratio of the mass of gas entering the boundary layer to the mass of gas remaining in the freestream increases. Two ways to increase this mass ratio are to decrease the pressure or decrease the tube radius. Decreasing pressure will enhance boundary layer growth while decreasing the tube radius will decrease the mass of the freestream gas so that the boundary layer growth is unaffected. A quantitative model designed to account for these effects

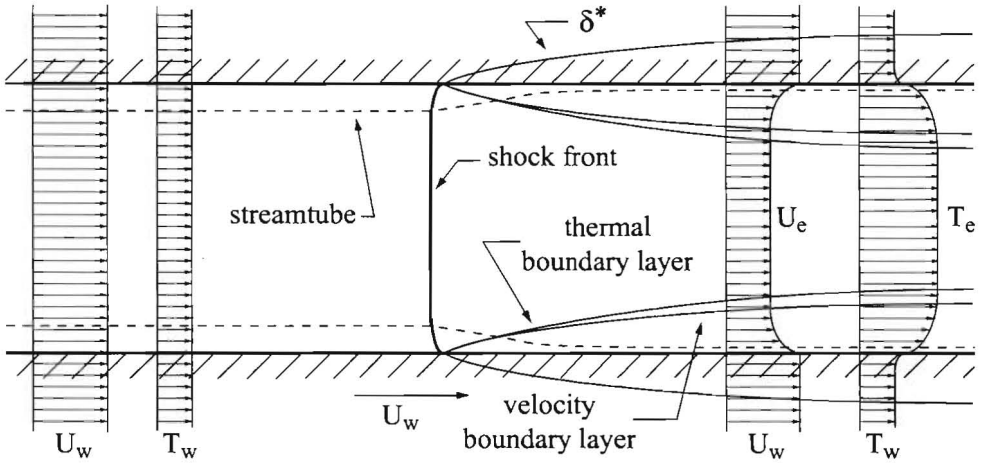

Figure 7: A shock wave propagating through a tube is shown in shock-fixed coordinates and illustrates the growth of the boundary layers and the displacement thickness. A streamtube, represented by the dashed line, illustrates the divergence of the flow behind the shock.

is discussed below.

4.2 Quasi-One-Dimensional Analysis for the Velocity Deficit of a Detonation Wave

The following derivation is taken from Dabora (1963) and presents a quasi-one-dimensional analysis for the velocity deficit of a detonation wave. First, the classical hydrodynamic formulation for the characteristics of a general, steady, one-dimensional wave with no area divergence will be discussed. This theory will then be adapted to allow for situations where area divergence is present behind the shock front. A solution will be developed to determine the velocity deficit resulting from this divergence. Applications of this solution by Fay (1959) and Dupre et al. (1986) will then be presented. Finally, those techniques will be applied to the current data.

4.2.1 One-Dimensional Waves with No Area Change

Modeling the wave as a one-dimensional planar discontinuity allows the conservation equations to be written in the following form:

$$\rho_1 w_1 = \rho_2 w_2 \tag{2}$$

$$\rho_1 w_1^2 + P_1 = \rho_2 w_2^2 + P_2 \tag{3}$$

$$\frac{w_1^2}{2} + h_1 = \frac{w_2^2}{2} + h_2 \tag{4}$$

where u, ρ, P, and h are the particle velocity, density, pressure, and enthalpy relative to the front. Conditions along the wave area are assumed to be uniform. The gases ahead and behind the wave can have different molecular weights m and ratios of specific heat γ; however, both gases are assumed to be thermally and calorically perfect. Thus, the equation of state is

$$P = \rho \frac{R_0 T}{m} \tag{5}$$

where R_0 is the universal gas constant and the enthalpy is defined as

$$h_1 = C_p T_1 = \frac{\gamma}{\gamma - 1} p_1 v_1 \tag{6}$$

$$h_2 = C_p T_2 - q = \frac{\gamma}{\gamma - 1} p_2 v_2 - q \tag{7}$$

where q is the heat release per unit mass due to chemical reaction.

Eqs. 2 and 3 can be combined to obtain the Rayleigh line:

$$\frac{\frac{P_2}{P_1} - 1}{\frac{v_2}{v_1} - 1} = -\frac{w_1^2}{P_1 v_1} = -\gamma_1 M_1^2 = -\frac{w_2^2 \rho_2^2}{P_1 \rho_1} \tag{8}$$

which forms a straight line with negative slope for any finite Mach number on a p-v diagram.

The Hugoniot relation can also be obtained by combining Eqs. 2, 3, 4, 6, and 7 and eliminating the velocity terms.

$$\left[\frac{2q}{P_1 v_1} + \frac{\gamma_1 + 1}{\gamma_1 - 1} - \frac{\gamma_2 - 1}{\gamma_2 + 1}\right]\left[\frac{\gamma_2 - 1}{\gamma_2 + 1}\right] = \left[\frac{P_2}{P_1} + \frac{\gamma_2 - 1}{\gamma_2 + 1}\right]\left[\frac{v_2}{v_1} - \frac{\gamma_2 - 1}{\gamma_2 + 1}\right] \tag{9}$$

On a p-v diagram, Eq. 9 represents a family of hyperbolas that are a function of the parameters q and γ.

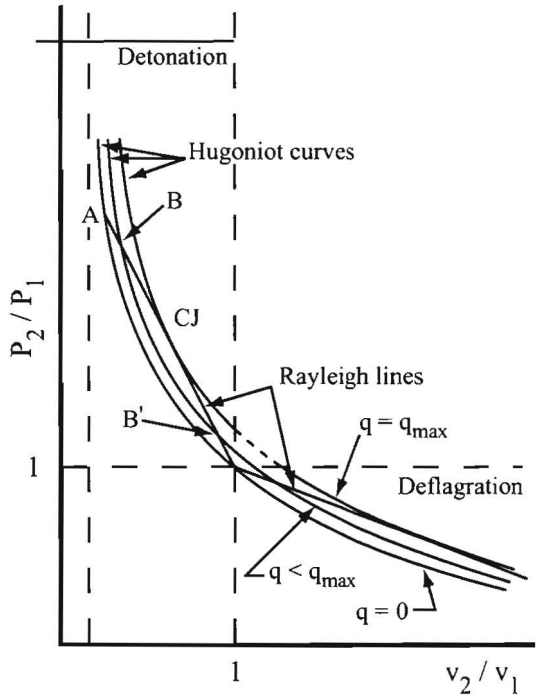

Figure 8: The Hugoniot-Rayleigh representation of shock and detonation waves.

Fig. 8 shows a schematic plot of Eq. 8 (two straight lines) and Eq. 9 for the adiabatic case and for two cases with heat release. The lower branch of the Hugoniot curves, in conjunction with Rayleigh lines of absolute slope less than γ_1, represent the deflagration mode of combustion and are not considered in this study. The upper branch of the Hugoniot and Rayleigh lines of absolute slope greater than γ_1 represent shock waves or detonation waves. In general, a Rayleigh line intersects the Hugoniot curve at two points, which represent the simultaneous solution of Eqs. 8 and 9. As an example, point A represents an adiabatic shock wave with P_2/P_1 and ρ_2/ρ_1 greater than unity. Point B is the solution for a strong detonation wave and point B' is that for a weak wave, both of which occur for values of q less than the limiting value. Points similar to B' are usually ruled out from entropy considerations if the detonation process is considered a shock followed by heat release. Finally, point CJ is the solution for the CJ wave and is realized at the limiting value of heat release. This is the type of wave observed in detonation tubes.

As can be seen from Fig. 8, at the CJ point, the Rayleigh line is tangent to the Hugoniot curve. Thus, it is possible to solve for this point by first differentiating Eqs. 8 and 9 to obtain

$$\frac{\partial\left(\frac{P_2}{P_1}\right)}{\partial\left(\frac{v_2}{v_1}\right)} = -\frac{w_2^2\rho_2^2}{P_1\rho_1} \tag{10}$$

and

$$\frac{\partial\left(\frac{P_2}{P_1}\right)}{\partial\left(\frac{v_2}{v_1}\right)} = -\frac{\frac{P_2}{P_1}+\frac{\gamma_2-1}{\gamma_2+1}}{\frac{\rho_1}{\rho_2}-\frac{\gamma_2-1}{\gamma_2+1}} \tag{11}$$

respectively.

Then, by equating Eqs. 10 and 11, substituting P_1 from Eq. 3 and w_1 from Eq. 2, the solution of w_2 for the CJ point is obtained:

$$w_2 = \sqrt{\frac{\gamma_2 P_2}{\rho_2}} = a_2 \tag{12}$$

which shows that for a CJ wave, the burned gas immediately behind the wave travels at the local sonic speed with respect to the wave.

With this CJ criterion, the jump conditions can be solved with the perfect gas relations to find the propagation velocity of the CJ detonation wave

$$M_{CJ} = \sqrt{\mathcal{H}+\frac{(\gamma_1+\gamma_2)(\gamma_2-1)}{2\gamma_1(\gamma_1-1)}} + \sqrt{\mathcal{H}+\frac{(\gamma_2-\gamma_1)(\gamma_2+1)}{2\gamma_1(\gamma_1-1)}} \tag{13}$$

where the non-dimensional heat of combustion $\mathcal{H}$ is given by

$$\mathcal{H} = \frac{(\gamma_2-1)(\gamma_2+1)q}{2\gamma_1 R_1 T_1} \tag{14}$$

and is typically of order 10 (Thompson, 1988). Eq. 13 is referred to as the two-γ CJ model.

The thermodynamic properties at the CJ surface can be determined by substitution into the conservation equations as well (Thompson, 1988)

$$\frac{P_2}{P_1} = \frac{\gamma_1 M_{CJ}^2 + 1}{\gamma_2 + 1} \tag{15}$$

$$\frac{\rho_2}{\rho_1} = \frac{\gamma_1(\gamma_2+1)\, M_{CJ}^2}{\gamma_2\,(1+\gamma_1 M_{CJ}^2)} \tag{16}$$

$$\frac{T_2}{T_1} = \frac{R_1}{R_2}\frac{P_2}{P_1}\frac{\rho_1}{\rho_2}\,. \tag{17}$$

Thus, if the initial thermodynamic conditions, as well as the value of heat release and γ_2 are known, the detonation velocity can be found. In general, however, finding q and γ_2 requires a trial and error solution that involves chemical equilibrium behind the wave. The equilibrium code STANJAN (Reynolds, 1986) is used in the present work.

A one-γ model is also available that uses a single specific heat ratio and perfect gas constant for both the reactants and products

$$M_{CJ} = \sqrt{\mathcal{H}+1} + \sqrt{\mathcal{H}}\,, \tag{18}$$

where $\mathcal{H}$ is identical to Eq. 14 with $\gamma_2 = \gamma_1$. Similarly, the thermodynamic properties are given by Eqs. 15-17 with $\gamma_2 = \gamma_1$ (Fickett and Davis, 2001).

4.2.2 One-Dimensional Waves with Area Change

For situations where there is an increase in stream-tube area between the shock wave and the CJ plane, a deficit in the propagation velocity will result. This type of situation occurs during boundary layer growth

as well as in the presence of an expanding tube diameter or yielding walls. Under these conditions, it is necessary to modify the conservation equations to account for the change in stream-tube area.

Defining the change in stream-tube area as

$$\frac{A_2}{A_1} = 1 + \xi \tag{19}$$

where ξ is the average fractional change in the area of each stream tube, the conservation equations become

$$\rho_1 w_1 = \rho_2 w_2 \left(1 + \xi\right) \tag{20}$$

$$\rho_1 w_1^2 + P_1 = \left(\rho_2 w_2^2 + P_2\right)\left(1 + \xi\right) - \int_0^{\xi} P \, d\xi \tag{21}$$

$$\frac{w_1^2}{2} + h_1 + q = \frac{w_2^2}{2} + h_2 \, . \tag{22}$$

The last term in Eq. 21 comes from considering the pressure force acting on the sides of the stream tube as it deforms behind the shock front. Evaluation of this term requires detailed knowledge of the pressure behind the shock front along the stream-tube boundary within the reaction zone. Fay (1959) chose to define the integral as

$$\int_0^{\xi} P \, d\xi \equiv P_2 \, \epsilon \, \xi \tag{23}$$

and noted that for large M_1, the ratio P_2/P_1 for a shock is about twice that for a detonation wave, so the value of ϵ is between 2 and 1.

Using the same general assumptions as for the case involving no area increase, Eqs. 20, 21, 22, and 23, together with the definition of the speed of sound, can be combined to give

$$2\left[1 + \frac{q}{c_{p_1} T_1}\right] = \left[\frac{\gamma_2}{\gamma_1}\right]^2 \left[\frac{\gamma_1 - 1}{\gamma_2^2 - 1}\right] \left(\frac{1}{1 - \frac{\xi\epsilon}{(1+\gamma_2)(1+\xi)}}\right)^2 \frac{\left(\gamma_1 M_1^2 + 1\right)^2}{M_1^2} - \left(\gamma_1 - 1\right) M_1^2 \, . \tag{24}$$

Introducing a new function ψ defined by

$$1 + \psi \equiv \left(\frac{1}{1 - \frac{\epsilon\xi}{(1+\gamma_2)(1+\xi)}}\right)^2 \tag{25}$$

allows Eq. 24 to be reduced to

$$2\left(\frac{q}{c_{p_1} T_1} - \frac{\gamma_1 - \gamma_2}{\gamma_1 \left(\gamma_2 - 1\right)}\right) \frac{\gamma_2^2 - 1}{\gamma_1 - 1} = \frac{\left(M_1^2 - \frac{\gamma_2}{\gamma_1}\right)^2}{M_1^2} + \frac{\psi \gamma_2^2 \left(M_1^2 + \frac{1}{\gamma_1}\right)^2}{M_1^2} \, . \tag{26}$$

The last term of this equation represents the effect of area change. For large M_1 (i.e., $M_1 \geq 5$), Eq. 26 can be reduced further:

$$2\left(\frac{q}{c_{p_1} T_1} - \frac{\gamma_1 - \gamma_2}{\gamma_1 \left(\gamma_2 - 1\right)}\right) \frac{\gamma_2^2 - 1}{\gamma_1 - 1} = M_1^2 \left(1 + \psi \gamma_2^2\right) \, . \tag{27}$$

If the heat release is assumed to remain the same whether there is an area change or not, the right-hand side of Eq. 27 remains essentially constant. Dabora (1963) notes that this is a reasonable assumption in that chemical equilibrium is expected to remain the same at the CJ plane whether there is an area

change or not. This is so because an area increase would decrease both pressure and temperature at that plane. The pressure decrease would increase the amount of radicals through increased dissociation and the lower temperature would slow the reaction rate. Thus, the pressure and temperature effects would tend to cancel each other, maintaining the amount of energy released in front of the sonic surface.

Noting that $\psi = 0$ when $\xi = 0$, one can find, after making use of Eq. 27, that the decrease in Mach number from the case where there is no area change ($\xi = 0$) to the case where ξ is finite can be written as:

$$\frac{M_1(\xi = 0) - M_1}{M_1(\xi = 0)} = \frac{\Delta M_1}{M_1(\xi = 0)} = 1 - \sqrt{\frac{1}{1 + \gamma_2^2 \psi}} \tag{28}$$

or in terms of ξ:

$$\frac{\Delta M_1}{M_1(\xi = 0)} = 1 - \sqrt{\frac{\left\{1 - \left[\frac{\epsilon}{1+\gamma_2}\right]\left[\frac{\xi}{1+\xi}\right]\right\}^2}{\left\{1 - \left[\frac{\epsilon}{1+\gamma_2}\right]\left[\frac{\xi}{1+\xi}\right]\right\}^2 + \gamma_2^2\left\{2\left[\frac{\epsilon}{1+\gamma_2}\right]\left[\frac{\xi}{1+\xi}\right] - \left[\frac{\epsilon}{1+\gamma_2}\right]^2\left[\frac{\xi}{1+\xi}\right]^2\right\}}} \tag{29}$$

which for $\xi \ll 1$ reduces to

$$\frac{\Delta M_1}{M_1(\xi = 0)} \cong \gamma_2^2 \left(\frac{\epsilon}{1+\gamma_2}\right) \xi \,. \tag{30}$$

This expression predicts the wave velocity deficit dependence on γ_2, ξ, and ϵ. Application of the solution involves choosing the appropriate values of these parameters.

4.2.3 Solution Application in Fay (1959)

Fay (1959) numerically calculated that for stoichiometric hydrogen-oxygen detonations at one atmosphere initial pressure,

$$\frac{\Delta M_1}{M_1(\xi = 0)} \cong 0.53 \epsilon \xi \,. \tag{31}$$

He then chose to express the fractional increase in stream-tube area ξ in terms of more convenient variables and approximated the increase in flow area as the displacement thickness times the tube circumference. Thus, the fractional area increase is approximately

$$\xi \simeq \frac{\pi d \delta^*}{\pi d^2/4} = \frac{4\delta^*}{d} \,. \tag{32}$$

Substituting Eq. 32 into Eq. 31 and approximating ϵ as 1, the expression for the velocity deficit becomes

$$\frac{\Delta M_1}{M_1} = \frac{\Delta U_1}{U_1} \simeq \frac{2.1\,\delta^*}{d} \tag{33}$$

where ΔU_1 is the difference between the observed detonation wave velocity and is normalized by the wave velocity in the divergence-free case U_1. For a detonation wave, U_1 is equal to the CJ velocity U_{CJ}. The equation used by Fay (1959) for displacement thickness was based on measurements (Gooderum, 1958) of turbulent boundary layers in shock tubes

$$\delta^* \simeq 0.22\, \ell^{0.8} \left[\frac{\mu_e}{\rho_1 U_{CJ}}\right]^{0.2} \,. \tag{34}$$

Gooderum (1958) initially reported the above expression for the growth of the turbulent boundary layer δ behind a shock in a shock tube. Analytical work by Fay (1959) argued that the expression could also be used for the displacement thickness δ^* behind the strong shock present in a detonation wave.

It is important to consider the value to use for the distance ℓ behind the shock when evaluating δ^*. Fay chose ℓ to equal the detonation wave thickness and determined this value by deriving a transcendental equation based on an experimental parameter he referred to as the relaxation length, which was obtained from experimental measurements of the density profile within a detonation front or from schlieren pictures.

In applying this model to the current experimental data, ℓ was set equal to the induction zone length Δ as calculated by CV (Shepherd, 1986), a resource not available to Fay in 1959. The initial gas density ρ_1 was known and the velocity U_{CJ} was computed using STANJAN (Reynolds, 1986). The post-shock gas viscosity μ_e was found not to vary significantly over the range of experimental conditions and was approximated as 6.0×10^{-5} Pa-s for the propane-oxygen mixtures tested.

The velocity predicted by this analysis is shown as a curve labeled "Fay" in Figs. 4c and 4d and in Figs. 6b, 6c and 6d. The predicted velocities agree very well with the experimental data in the 1.27 mm ID tube, but slightly under-predict the measured wave velocities in the 6.35 mm ID tube.

4.2.4 Solution Application in Dupre et al. (1986)

Dabora (1963) used a value of $\gamma_2 = 1.2$ for hydrogen-oxygen detonations to obtain a coefficient of 0.654 in Eq. 30 instead of the value of 0.53 numerically calculated by Fay (1959). However, Dabora (1963) also observed that in his applications, ξ could be as large as 0.25 and chose to use Eq. 29 instead of Eq. 30.

The model discussed in Dupre et al. (1986) used Eq. 29 with a definition for stream-tube area divergence developed by Murray (1984), which evaluated δ^* at a distance of one detonation cell length l_c downstream of the shock:

$$\xi = 4\frac{\delta^*_{l_c}}{d} \,. \tag{35}$$

The equation used for predicting velocity deficit was

$$\frac{\Delta U_1}{U_1} = 1 - \left[\frac{(1-\nu)^2}{(1-\nu)^2 + \gamma_2^2\,(2\nu - \nu^2)}\right]^{\frac{1}{2}} \tag{36}$$

where

$$\nu = \frac{\xi}{|\,(1+\gamma_2)\,(1+\xi)\,|} \,. \tag{37}$$

Eqs. 36 and 37 are identical to Eq. 29. Dupre et al. (1986) used Dabora's choice of $\gamma_2 = 1.2$ for H_2-O_2 mixtures and also chose $\ell = \lambda/0.7$ in their analysis where λ was the detonation cell width.

This model was used to predict velocity deficits in the experimental data in the present work. Eq. 34 was first used to compute the displacement thickness behind the shock wave with downstream distance $\ell = \lambda/0.7$. The initial density was known and the velocity U_{CJ} was determined according to CJ theory by using the equilibrium code STANJAN (Reynolds, 1986). As before, the viscosity of the gas behind the shock wave μ_e was approximated as 6.0×10^{-5} Pa-s.

Eq. 36 was then used with Eq. 35 and 37 to determine the expected velocity deficit. In this study, the value of $\gamma_2 = 1.14$ was used for the propane-oxygen mixtures.

The result is the line labeled "Dabora" in Figs. 4c, 4d, 6b, 6c. This model fits the data well in the 6.35 mm ID tube, but underpredicts the velocity deficits observed in the 1.27 mm ID tube.

4.2.5 Limitations of the Model

The quality of the fit can vary with the values of γ_2 used in each analysis. For example, as mentioned above, the value of γ_2 used in the "Dabora" line in Figs. 4 and 6 was $\gamma_{2_D} = 1.14$. The value of γ_2 used in the "Fay" line can be determined from setting the right-hand sides of Eqs. 30 and 31 equal to each other and solving for γ_2. The result is that $\gamma_{2_F} = 1.04$. Since γ_2 decreases with decreasing mixture pressure, it is possible that the model in Dupre et al. (1986) does not fit the high-deficit, low-pressure experimental data simply because the value of γ_2 used in the model is too large. Similarly, the model of Fay (1959) does not fit the high-pressure, low-deficit data well, but the fit improves as the mixture pressure (and thus γ_2) is decreased. Thus, it may be necessary to "tune" each model to a specific pressure range by selecting the appropriate value of γ_2.

A second factor to consider is that while the model generally predicts the velocity deficit trend, it does not fully account for the physics of boundary layer growing in the tube. For cases with low initial pressure, the boundary layer will completely close behind before the onset of the reaction zone. While it is not physically possible for the boundary layer to continue to remove mass from the freestream flow after it has completely closed, the model continues to do so since it was not designed to account for such situations. While the model appears to accurately predict deficits when the boundary layer closure distance is shorter than the induction length, this is just luck and the model is reduced to an empirical fit. The models based on frictional flow in a tube (Zel'dovich et al., 1987, Frolov and Gelfand, 1991, Agafonov and Frolov, 1994) may be more appropriate for these cases.

4.3 Lower Shock Velocity Limits

The strength of the shock that would be created in the test section when a detonation is successfully initiated in the initiator tube but fails during the transition to the test section (for large values of Δ/R) is estimated below. Predicting the maximum possible shock speed would help interpret the experimental data since no reaction zone information was collected. This situation is analyzed using a shock tube model and a blowdown model.

4.3.1 Shock Tube Model

The situation described above is modeled using a shock tube or unsteady wave analysis. Initially, the initiator and test-section tubes are filled with the same mixture at identical pressures. Assume the detonation wave in the initiator tube fails immediately upon entering the test-section tube. The pressure in the initiator tube will not be uniform as the reflections from the detonation wave from the tube end flanges interact with the Taylor wave; however, after the wave reflections have been allowed to run their course, the pressure in the detonation tube will be close to the constant volume combustion pressure P_{CV}.

The shock tube equation

$$\frac{P_{CV}}{P_1} = \frac{1 + \frac{2\gamma_1}{\gamma_1 + 1}({M_s}^2 - 1)}{(1 - \frac{\gamma_{CV} - 1}{\gamma_1 + 1}\frac{a_1}{a_{CV}}\frac{{M_s}^2 - 1}{M_S})^{\frac{2\gamma_{CV}}{\gamma_{CV}-1}}} \tag{38}$$

matches conditions across the shock wave and expansion fan to determine the Mach number M_s of the shock that is created in the test section. For stoichiometric propane-oxygen mixtures, the ratio of the constant volume explosion pressure to the initial pressure is approximately constant ($P_{CV}/P_1 \approx 18$) and the ratio of the local sound speeds before and after combustion ($a_{CV}/a_1 \approx 3.9$). The ratio of specific heats for a stoichiometric propane-oxygen mixture is $\gamma_1 = 1.29$, which changes after combustion to $\gamma_{CV} \approx 1.12$ assuming equilibrium composition.

Substituting the aforementioned values into Eq. 38 yields $M_s \approx 2.9$. The typical initial test section sound speed a_1 and U_{CJ} are approximately 308 m/s and 2300 m/s, respectively. This indicates that,

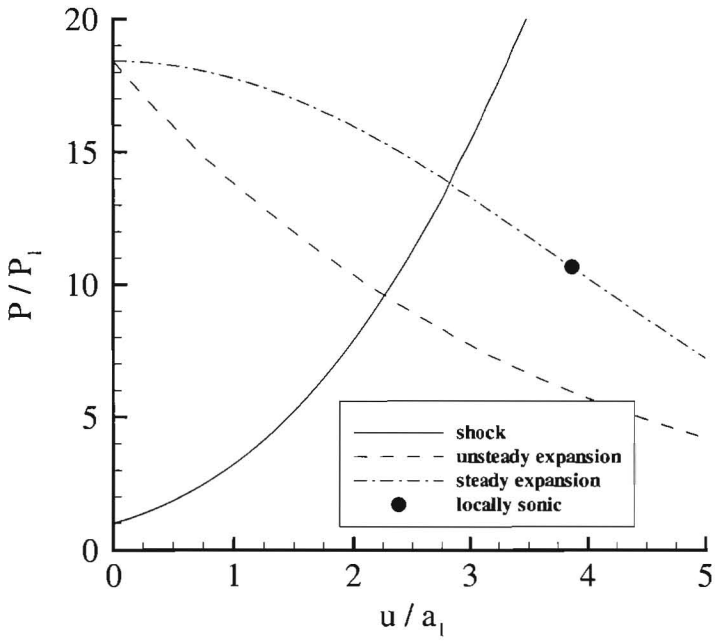

Figure 9: A graphical illustration of the difference between steady and unsteady expansion. The intersection of the shock and unsteady expansion lines represents the solution of the shock tube equation. The intersection of the shock and steady expansion lines represents the solution corresponding to quasi-steady flow expansion.

neglecting boundary layer losses, a non-reacting shock wave would propagate through the test section at a wave speed U_s of 890 m/s, and a normalized velocity value U_{AVG}/U_{CJ} of 0.39. This velocity is slightly below the lowest velocities measured in the 1.27 mm ID tube (Fig. 6b).

4.3.2 Blowdown Analysis

If the driver tube has a significantly larger diameter than the test section tube (as in this experiment), the initial shock wave in the test section will be created by the unsteady phenomenon mentioned in the previous section, but will transition to a quasi-steady solution for longer times. The initial pressure difference between the initiator and test section tubes when the detonation reaches the end of the initiator tube drives fluid into the test section, creating a shock in the test section and expansion waves in the initiator. However, as the expansion waves diffract into the much larger initiator tube volume, they weaken significantly and the stagnation conditions inside the driver change slowly relative to the time-scale of interest, the propagation time of the shock wave in the test section tube. Thus, the process can be approximated as steady, and isentropic analysis can be used.

Assuming negligible heat losses, a steady flow accelerating the gas from the initiator tube into the test section can be modeled as adiabatic. Thus, the stagnation enthalpy is constant at the CV condition

$$h_{CV} = h(t) + \frac{u(t)^2}{2} . \tag{39}$$

For a perfect gas,

$$\Delta h = c_p \, \Delta T \tag{40}$$

making the temperature ratio

$$\frac{T(t)}{T_{CV}} = 1 - \frac{(\gamma - 1)}{2} \frac{u(t)^2}{a_{CV}^2} \, . \tag{41}$$

Assuming the flow is smoothly accelerated from the driver into the test section, the flow in the transition from the driver to the test section can be modeled as an isentropic expansion and the pressure ratio can be computed as

$$\frac{P(t)}{P_{CV}} = \left(\frac{T(t)}{T_{CV}} \right)^{\frac{\gamma}{\gamma - 1}} \tag{42}$$

$$\frac{P(t)}{P_{CV}} = \left[1 - \frac{(\gamma - 1)}{2} \frac{u(t)^2}{c_{CV}^2} \right]^{\frac{\gamma}{\gamma - 1}} \, . \tag{43}$$

Eq. 43 represents the range of pressure-velocity values that may exist in the initiator tube due to isentropic expansion. In reality, the flow is not perfectly isentropic, resulting in lower pressures experimentally than predicted by isentropic theory.

In order to choose a specific set of pressure and velocity values, it is necessary to solve the intersection of Eq. 43 with the equation for the pressure increase across a shock wave:

$$\frac{P_2}{P_1} = 1 + \frac{2\gamma_1}{\gamma_1 + 1} \left(M_s^2 - 1 \right) \, . \tag{44}$$

Doing so will match the pressure and velocity at the interface between the shocked test section gas and the expanding initiator tube flow.

This solution is illustrated graphically in Figs. 9. The steady expansion curve intersects the shock curve at a pressure of $P_2/P_1 = 13.8$. This corresponds to a shock Mach number of 3.5 and a shock speed of 1077 m/s. The intersection occurs before the expanded flow is locally sonic indicating that this is a valid solution. A shock interpreted as a detonation wave would have a U_{AVG}/U_{CJ} value of approximately 0.46 for the range of conditions investigated. Examination of the data (Fig. 6) shows that there is only one data point below this value, indicating that a reaction zone was most likely present in the test section for all other cases.

5 Summary

Detonation waves were propagated in propane-oxygen mixtures through tubes with diameters of 6.35 mm and 1.27 mm, which are on the order of the detonation cell size. For experiments in the 6.35 mm ID tube, initial pressure and equivalence ratio were varied. Stoichiometric propane-oxygen mixtures were tested with initial pressures varying from 0.1 to 1 bar, and the mixture equivalence ratio ϕ was varied from 0.3 to 3. For experiments in the 1.27 mm ID tube, the initial pressure of stoichiometric propane-oxygen mixtures was varied from 0.1 to 1.8 bar.

Wave speeds in the test section were found to decrease significantly below the CJ velocity as the initial pressure decreased. Minimum propagation velocities of 0.4 U_{CJ} were observed for mixtures with initial pressures of 0.14 bar. Velocity deficits were also measured as ϕ diverged from unity. The measured velocity data normalized by U_{CJ} appear to collapse to a single relationship dependent on induction zone length normalized by the tube radius. The induction zone length of each test mixture was calculated based on the initial state and the experimentally measured wave speed.

Deficits in the detonation wave velocity were attributed to boundary layer growth. A boundary layer model was used to quantitatively predict the decrease in detonation wave velocity as a function of a given tube diameter, initial gas properties and the parameters γ_2, ξ, and ϵ. Two versions of the model with different choices of parameters were used to predict the experimental data.

The first version from Fay (1959) substituted the induction zone length in place of Fay's original choice of relaxation length to calculate the displacement thickness and resulting stream-tube divergence. This model was found to agree well with the experimental data from the 1.27 mm ID tube where significant velocity deficits below 0.9 U_{CJ} were present, but underpredicted the velocities measured in the 6.35 mm ID tube.

The second version presented in Dupre et al. (1986) was also based on Fay's model with contributions from Dabora (1963) and Murray (1984). This model was found to accurately predict velocities in the 6.35 mm ID tube, but overpredicted wave velocities in the 1.27 mm ID tube. Since data from the 6.35 mm ID tube typically had small velocity deficits (less than 10% of U_{CJ}) and data from the 1.27 mm ID tube had larger velocity deficits (15% to 60% of U_{CJ}), it seems that the version of Fay (1959) better predicts situations where large velocity losses are present, while the modified model (Dupre et al., 1986) works better for smaller losses.

The choice of γ_2 can significantly affect the fit of the model to the experimental data, and decreasing the value of γ_2 as mixture pressure is decreased would improve the fit of each model. Additionally, it is important to be aware that the model does not account for situations where the boundary layer closes before the end of the reaction zone.

Experimental diagnostics such as ionization gauges were not present to measure the reaction zone trajectory in the tube, so it is possible that the detonation waves failed at the lowest speeds. This would have resulted in shock waves in the test section being interpreted as detonation waves with large velocity deficits. Unsteady and quasi-steady wave analyses were used to predict the maximum propagation velocity of a shock wave in this situation, assuming that pressure in the initiator tube corresponded to the constant volume explosion pressure. The maximum expected shock propagation velocity was calculated to be 0.46 U_{CJ}, which was close to the slowest observed wave propagation velocities in the test section. The experiments showed that the wave velocities did not decay as the waves propagated through the test section. This suggests that it is unlikely that detonation failure in the test section was responsible for the observed velocity deficits.

Future experimental work should include a larger range of test section tube diameters to verify the effect of tube diameter on propagation velocity and enable further model development. Additionally, in future experiments, more care should be taken to ensure that the ID of each test section remains constant and free of obstacles that could enhance DDT or disrupt the detonation wave. Extending the length of each test section to several thousand tube diameters would help identify whether the observed velocity deficits were the result of a failing wave or a steady state process.

Also, the initiator tube should be modified to successfully initiate a detonation wave but not to act as a piston pushing on the test section gas. One way to do this would be to allow the initiator tube to vent pressure to the atmosphere behind the detonation wave. In the event of detonation failure in the test section, this would prevent a strong shock from being supported in the test section. Future experiments should detect the location of the reaction zone relative to the shock wave. Photodiodes or ionization probes located at the same axial location as the pressure transducer would confirm the presence of combustion and would allow direct measurement of the distance between the shock wave and the reaction zone.

References

G.L. Agafonov and S.M. Frolov. Computation of the detonation limits in gaseous hydrogen-containing mixtures. *Combustion, Explosion, and Shock Waves*, 30(1):91–100, 1994.

I. Brailovsky and G. Sivashinsky. Hydraulic resistance and multiplicity of detonation regimes. *Combustion and Flame*, 122(1-2):130–138, 2000.

I. Brailovsky and G. Sivashinsky. Effects of momentum and heat losses on the multiplicity of detonation regimes. *Combustion and Flame*, 128(1-2):191–196, 2002.

M. Brouillette. Shock waves at microscales. *Shock Waves*, 13:3–12, 2003.

E.K. Dabora. *The Influence of a Compressible Boundary on the Propagation of Gaseous Detonations.* PhD thesis, University of Michigan, Ann Arbor, Michigan, 1963.

J.P. Dionne, H.D. Ng, and J.H.S. Lee. Transient development of friction-induced low-velocity detonations. In *Proceedings of the Combustion Institute*, volume 28, pages 645–651. The Combustion Institute, 2000.

J.E. Dove, B.J. Scroggie, and H. Semerjian. Velocity deficit and detonability limits of hydrogen-oxygen detonations. *Acta Astronautica*, 1:345–359, 1974.

G. Dupre, R. Knystautas, and J.H. Lee. Near-limit propagation of detonation tubes. *Progress in Astronautics and Aeronautics*, 106:244–259, 1986.

D.H. Edwards, G. Hooper, and R.J. Meddins. Microwave velocity measurements of marginal detonation waves. *Journal of Physics D - Applied Physics*, 3(7):1130–1134, 1970.

D.H. Edwards, G. Hooper, and J.M. Morgan. A study of unstable detonations using a microwave interferometer. *Journal of Physics D - Applied Physics*, 7:242–248, 1971.

J.A. Fay. Two-dimensional gaseous detonations: Velocity deficit. *The Physics of Fluids*, 2(3):283–289, May-June 1959.

W. Fickett and W.C. Davis. *Detonation Theory and Experiment.* Dover Publications Inc., Mineola, New York, 2001.

S.M. Frolov and B.E. Gelfand. Limit diameter of gas detonation propagation in tubes. *Combustion, Explosion, and Shock Waves*, 27(1):113–117, 1991.

P.B. Gooderum. An experimental study of the turbulent boundary layer on a shock-tube wall. NACA Tech. Note 4243, NACA, 1958.

F. Haloua, M. Brouillette, V. Lienhart, and G. Dupre. Characteristics of unstable detonations near extinction limits. *Combustion and Flame*, 122:422–438, 2000.

R. J. Kee, F. M. Rupley, and James A. Miller. CHEMKIN-II: A Fortran chemical kinetics package for the analysis of gas-phase chemical kinetics. Technical Report SAND89-8009, Sandia National Laboratories, 1989.

G.B. Kistiakowsky and W.G. Zinman. Gaseous detonations. vii. a study of thermodynamic equilibration in acetylene-oxygen waves. *The Journal of Chemical Physics*, 23(10):1889–1894, October 1955.

G.B. Kistiakowsky, H.T. Knight, and M.E. Malin. Gaseous detonations. III. Dissociation energies of nitrogen and carbon monoxide. *The Journal of Chemical Physics*, 20(5):876–883, May 1952a.

G.B. Kistiakowsky, H.T. Knight, and M.E. Malin. Gaseous detonations. IV. The acetylene-oxygen mixtures. *The Journal of Chemical Physics*, 20(5):884–888, May 1952b.

J.J. Lee, G. Dupre, R. Knystautas, and L.H. Lee. Doppler interferometry study of unstable detonations. *Shock Waves*, 5(3):175–181, 1995.

B. Lewis and G. von Elbe. *Combustion, Flames and Explosions of Gases.* Academic Press, Second Edition, 1961.

V.I. Manzhalei. Detonation regime of gases in capillaries. *Combustion, Explosion and Shock Waves*, 28 (3):296–302, 1992.

V.I. Manzhalei. Low-velocity detonation limits of gaseous mixtures. *Combustion, Explosion, and Shock Waves*, 35(3):296–302, 1999.

S.B. Murray. *The Influence of Initial and Boundary Conditions on Gaseous Detonation Waves.* PhD thesis, McGill University, McGill, Canada, 1984.

C. Paillard, G. Dupre, R. Lisbet, J. Combourieu, V.P. Fokeev, and L.G. Gvozdeva. A study of hydrogen azide detonation with heat transfer at the wall. *Acta Astronautica*, 6:227–242, 1979.

W. C. Reynolds. The element potential method for chemical equilibrium analysis: Implementation in the interactive program stanjan, version 3. Technical report, Dept. of Mechanical Engineering, Stanford University, Stanford, CA, 1986.

E. Schultz. *Detonation Diffraction Through an Abrupt Area Expansion.* PhD thesis, California Institute of Technology, Pasadena, CA, 2000.

G.J. Sharpe. Numerical simulations of pulsating detonations: Ii. piston initiated detonations. *Combustion Theory and Modelling*, 5:623–638, 2001.

J.E. Shepherd. Chemical kinetics and cellular structure of detonations in hydrogen sulfide and air. In *Prog. Astronaut. Aeronaut.*, volume 106, pages 294–320, 1986.

A. Teodorczyk, J.H.S. Lee, and R. Knystautas. Propagation mechanism of quasi-detonations. In *22nd Symposium (International) on Combustion*, pages 1723–1731. The Combustion Institute, 1988.

P.A. Thompson. *Compressible-Fluid Dynamics.* McGraw-Hill, New York, 1988.

A. Vasil'ev. Geometric limits of gas detonation propagation. *Combustion, Explosion, and Shock Waves*, 18(2):245–249, 1982.

Y.B. Zel'dovich, B.E. Gelfand, Y.M. Kazhdan, and S.M. Frolov. Detonation propagation in a rough tube taking account of deceleration and heat transfer. *Combustion, Explosion, and Shock Waves*, 23 (3):342–349, 1987.